Modeling of Polymer Crystallization in a Temperature Gradient

Ewa Piorkowska

Centre of Molecular and Macromolecular Studies, Polish Academy of Sciences, Sienkiewicza 112, 90-363 Lodz, Poland

Received 25 April 2001; accepted 11 February 2002

ABSTRACT: The crystallization of polymer films in a temperature gradient was simulated. The curvature of lamella growth directions observed experimentally was taken into account. The computer simulation permitted the visualization of the evolution of the spherulitic pattern and also the calculation of the conversion of the melt into spherulites. The mathematical model was also elaborated and allowed the prediction of the kinetics of conversion during the crystallization of polymers in the temperature gradient. A good agreement between the computer simulation results, the mathematical model predictions, and the experimental data for isotactic polypropylene crystallized in a temperature gradient was obtained. © 2002 Wiley Periodicals, Inc. J Appl Polym Sci 86: 1351–1362, 2002

Key words: crystallization; isotactic poly(propylene); modeling; temperature gradient

INTRODUCTION

The low thermal conductivity of polymers results in a slow heat subtraction from thick-wall products cooled and solidified during industrial processes. The liberation of the heat of crystallization is an additional factor causing slower cooling or even an increase in temperature inside such objects.[1] Therefore, the solidification of polymers occurs in temperature gradients.

The temperature dependencies of both the spherulite nucleation and growth rate result in significant differences in the crystallization kinetics and in the final spherulite structure between regions solidifying at different temperatures. It is also known that the temperature gradient leads to anisotropic spherulite growth and shapes and affects the directions of spherulite growth. The growth trajectories bend in the temperature gradient, being normal to the growth front.[2–4] The changes in interspherulitic boundary shapes have also been reported.[2,4] Recently, Pawlak and Piorkowska[4] showed that the temperature gradient could accelerate the conversion of the melt into spherulites.

Correspondence to: E. Piorkowska (epiorkow@bilbo.cbmm.lodz.pl).

Contract grant sponsor: Polish State Committee for Scientific Research through the Centre of Molecular and Macromolecular Studies (PAS); contract grant number: 7 T08E 016 12.

Journal of Applied Polymer Science, Vol. 86, 1351–1362 (2002)

Besides experiments, the modeling of crystallization also provides insight into the development and final form of the spherulitic structure. The modeling of spherulitic crystallization concerned mainly the processes occurring in a uniform temperature field. The conversion of the melt into crystalline domains growing from random nuclei was first described by Evans,[5] who calculated the probability that an arbitrarily chosen point remained unoccluded by spheres or circles expanding radially from nuclei distributed randomly in the sample. Avrami[6] introduced the concept of extended volume, the total volume of all domains growing from all nuclei, including phantom events in the already crystallized area and neglecting the truncation. Both approaches are equivalent and based on the assumption that only the first domains passing through sampling points are real and still growing because domains that have originated from phantoms and domains truncated by neighbors are delayed. Therefore, the conversion degree at a certain time t is expressed by the classic equation, $\alpha(t) = 1 - \exp[-E(t)]$, with E denoting the extended volume or expectancy. An earlier treatment of the problem by Kolmogoroff[7] is based on an inaccurate approach: the errors made in his derivation accidentally cancel one another, leading to the correct result.[8]

The results of the computer simulation of spherulitic growth from nuclei[9] agree with the Avrami theory; however, many authors have pointed out the reasons for discrepancies between the experimental results and the theoretically predicted value of the Avrami exponent.[10]

Later development of the theory permitted the expectancy, $E(t)$, to be obtained for a time-dependent

nucleation rate[11] and for the problem of the temperature-dependent nucleation and growth rate but with the additional assumption that the temperature changes linearly with time.[12] The effects of finite sample sizes and surface nucleation were also evaluated.[11,13–15]

In the general Avrami approach,[6] the extended volume around a certain point of a sample, A, equals the average number of extended domains that have grown through point A. Therefore, it is the integral of the time- and position-dependent nucleation rate, F, over the so-called region of influence of A:

$$E(t, A) = \int_0^{\pi} \int_0^{2\pi} \int_0^{R} \left[\int_0^{t'} F(\tau, r, \theta, \varphi)\, d\tau \right] \times r^2 \sin\theta\, dr\, d\varphi\, d\theta \quad (1)$$

where τ is the time; r, θ, and ϕ are spherical coordinates about A as the origin; and t' denotes the nucleation time for the domain nucleated at position r,θ,ϕ and passing through point A exactly at time t. Time t' is determined by the differential equation, $d\rho = -G_s(\tau,r,\theta,\phi)d\tau$, fulfilling the conditions $\tau = t$ at $\rho = 0$ and $\tau = t'$ at $\rho = r$, where G_s denotes the time- and position-dependent growth rate of domains. $R(\theta,\phi,t)$ is the radius at t of the domain that was nucleated at $t' = 0$ at θ,ϕ and reached point A at time t: $R = r$ for $t' = 0$. In principle, eq. (2) permits us to describe the kinetics of crystallization in complicated conditions, although no application of that formula was demonstrated in ref. 6.

The approach developed by Piorkowska and Galeski[16,17] and Piorkowska[18,19] was based on the concept of nucleation attempts as random events in space and time. It allows not only for the evaluation of the conversion degree of the melt into domains but also for the description of the structure formation process and the final microdomain pattern for both isothermal and nonisothermal conditions in infinite and finite samples. The possibility of including the dependence of the nucleation rate and spherulite growth rate on time and position was pointed out in ref. 16, leading, however, to eq. (1).

The computer simulation of spherulitic structure formation allows us to follow the evolution of the spherulite pattern, including the determination of the overall crystallization kinetics. Although the radial growth of spherulites was a basic assumption in all existing mathematical models of overall crystallization kinetics, the changes in lamella growth directions were first taken into account in computer modeling by Lovinger and Gryte.[20] The calculations, however, were limited to the prediction of the quasi-parabolic shape of a single spherulite occluded by a unidirectionally growing crystallizing front in poly(ethylene oxide).

Shulze and Naujack[3,21] derived an analytical equation describing the anisotropic shape of the spherulite and the variable growth directions in a uniaxial field of the growth rate by introducing the condition of the minimum time along the growth lines. The growth lines were always normal to the growth front. The obtained results were verified by comparison with the data for the crystallization of isotactic polypropylene (iPP) in the temperature gradient of 8–11 K mm^{-1}.

Recently, the multiscale model for polymer crystallization was described by Charbon and Swaminarayan.[22,23] The arborescent technique allowed them to follow the growth of individual fibrils within a spherulite. The necessity of performing a large number of computations limited the applicability of this method, and so the second technique, front tracking, based on the tracking of the crystallization front evolution, was elaborated. The front tracking method, based on the growth normal to the growth front, was combined with the solution of the heat conduction equation and was applied for the prediction of polyethylene spherulitic structure development in a plate cooled by contact with a mold at constant temperature. The spherulite nucleation and growth were considered in two dimensions. Despite other simplifications of the problem, such as the regimes of the growth rate being neglected, the results gave an idea of the possible structure transformation induced by the temperature gradient, including the change in the growth direction of lamellae.

Although the two-dimensional model is not representative of the crystallization in bulk, the application of the described methods of modeling to bulk crystallization seems rather difficult because of the necessity of following the trajectories of growth-front points in three dimensions. However, the temperature gradient can accelerate the conversion of the melt into spherulites,[4] and so considering the conversion rate to be dependent only on the local temperature can lead to erroneous results. In refs. 22 and 23, no data concerning the overall kinetics of crystallization are presented The changes in the temperature field with time do not allow determination of the effect of the temperature gradient at different local temperatures on the final spherulitic structure.

In this article, the spherulitic crystallization of iPP film is modeled in a uniaxial linear temperature field. The evolution of shapes of individual spherulites and the entire spherulitic pattern in a constant temperature gradient was computer-simulated. The conversion of the melt into spherulites in the temperature gradient was also computed. The probabilistic model is described and allows us to predict the conversion of the melt into spherulites during gradient crystallization in

two and three dimensions. In the analytical model, the radial growth of lamellae is assumed. For the determination of the error introduced by this assumption, the computer simulation of spherulite growth was conducted for two cases: radial growth and growth normal to the crystallization front. The effects of the local temperature, the temperature gradient, and the nucleation density on the kinetics of crystallization are demonstrated. Both the computer simulation and the analytical model are verified by a comparison of the results with the experimental data of Pawlak and Piorkowska.[4]

COMPUTER SIMULATION

The two-dimensional crystallization of iPP in a uniaxial linear temperature field was computer-simulated. The evolution of single iPP spherulites and interspherulitic boundaries between neighboring spherulites, as well as the resulting spherulitic patterns consisting of spherulites growing from randomly distributed nuclei, were simulated.

The well-known dependence of the iPP spherulite growth rate, g, on the crystallization temperature, T,[24] was applied:

$$g(T) = G_0 \exp\{-U[R(T - T_\infty)]^{-1}\} \exp\{-K_g[T(T_m^0 - T)]^{-1}\} \quad (2)$$

where $U = 1500$ cal mol^{-1}, $T_\infty = 231.2$ K, and $T_m^o = 458.2$ K, whereas G_0 and K_g depend on the regime of crystallization for a given iPP. The values of K_g and G_0 were used as determined experimentally[25,26] for Polysciences iPP, with a weight-average molecular weight (M_w) of 220,000: 1.47×10^5 K^2 and 0.3359 cm s^{-1} in regime II ($T \geq 136$°C) and 3.30×10^5 K^2 and 3249 cm s^{-1} in regime III ($T \leq 136$°C) The depression of g due to fractionation[26] or due to negative pressure buildup in occluded pockets of melt[26,27] was not taken into account. $g(T)$ was recalculated for the growth-rate dependence on the x coordinate, $G(x)$, with the relation describing the linear temperature distribution: $T = T_0 + \Lambda x$.

Points at spherulite circumferences were displaced in subsequent time intervals by the distance equal to the product of the time interval and the growth rate as determined by the local temperature according to eq. (2). Two models of spherulite growth were considered: (1) radial growth and (2) variable growth directions always normal to the growth front. The growth-front points entering the area already occupied by other spherulites were rejected. In the probabilistic model of spherulitic nucleation and growth, the first growth front passing through a sampling point was always considered real, independently of what happened earlier, and so in the computer simulation of radial propagation, the growth along trajectories emerging from other spherulites was reactivated. For the model of the variable growth direction, the growth along the trajectory entering the region occupied earlier by other spherulite stopped.

The spherulitic samples were rectangles in which the positions of spherulite nuclei were randomly chosen by means of a subtract-with-borrow pseudorandom number generator, $Z_n = Z_{n-10} - Z_{n-24} - c \bmod (2^{24})$, described in ref. 28. All spherulites started to grow simultaneously from nuclei at the beginning of crystallization. The crystallization processes were simulated (1) with a constant nucleation density and (2) with the nucleation density dependent on temperature. In general, the nucleation is related to the crystallization temperature, but treating it as a constant across the sample permitted the influence of the variable G to be demonstrated on the process of formation and the final form of the spherulitic pattern. For temperature-dependent nucleation density, the pseudorandom number generation method of von Neumann[29] was applied. Two types of temperature relationships of nucleation density were considered: (1) proportional to G and (2) determined experimentally for Polyscience iPP ($M_w = 220{,}000$), where the number of spherulite centers per cubic millimeter of the polymer, at the crystallization temperature T (°C), was approximated by the following formula:[4]

$$I = \exp[111.265 - 0.2544(T + 273.15)] \quad (3)$$

The conversion degree was calculated at selected isotherms passing through samples containing at least 200 spherulites, and 2000 points equally spaced along the isotherm were chosen in each sample. In subsequent time intervals, the fraction of the total number of these points occupied already by growing spherulites was computed. Care was taken to ensure the proper distances from selected isotherms to the sample boundaries to exclude the influence of the finite sizes of samples on obtained results. Several samples were simulated for each crystallization process until no significant influence of an additional data set on averaged results was observed. The spherulitic crystallization in different temperature gradients, Λ, and also in the uniform temperature field was simulated. In the last case, the variable-growth-direction model and the radial-growth model led to the exactly the same results.

PROBABILISTIC MODEL

The probabilistic approach elaborated and described previously in refs. 16–18 is applied here to describe spherulitic crystallization in the temperature gradient.

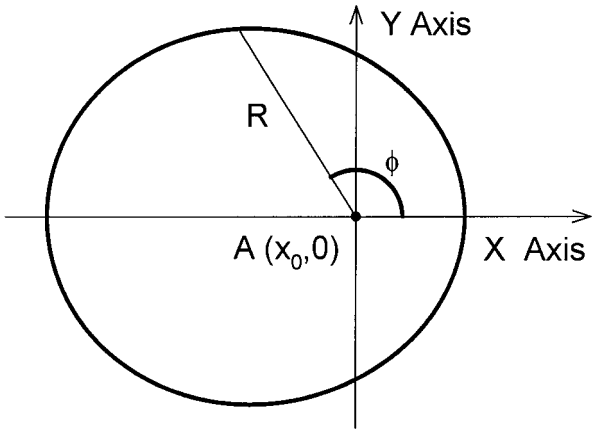

Figure 1 Point A on the plane.

It is assumed that the temperature increases linearly in the x direction, and so the isotherms are parallel to the y axis, and that the spherulites are nucleated instantaneously at the beginning of the crystallization process. The considerations that follow are based on the assumption that spherulite nucleation can be described as a set of random attempts occurring on a plane and creating radially expanding circles. For simplification of the problem, the radial spherulite growth is assumed. The local nucleation density, D, denotes the average number of nucleation attempts per unit area. At any sample point, only the first arriving circle is considered because it represents a real growing spherulite. In general, the nucleation density and the spherulite growth rate depend on the temperature, but in a known unidirectional temperature field, they can be treated as dependent on a spatial coordinate: $D = D(x)$ and $G = G(x)$. Isothermal crystallization is then a particular process with G a constant.

An arbitrarily chosen point, A(x_0,0), on a plane (Fig. 1) will remain unoccluded by spherulites until time t elapsed from the beginning of crystallization if no spherulite is nucleated within the certain area, $S(t)$, with the following properties. The zone $S(t)$ is defined by the anisotropic growth of virtual spherulites nucleated on its circumference that would arrive at point A at time t; that is, those spherulites would have the radius $R(\phi,t)$ measured in the direction toward point A. As it follows from the derivations described in refs. 16–19, the probability that no nucleation event occurs in the area, S, equals $\exp(-E)$, where E is the integral of D over $S(t)$:

$$E(x_0, t) = \int_S D\, ds \tag{4a}$$

The conversion degree of the melt into spherulites, α, is given by the following equation:

$$\alpha(x_0, t) = 1 - \exp[-E(x_0, t)] \tag{4b}$$

During time t, the spherulite radius increases from 0 to $R(\phi,t)$. One can, therefore, calculate time t as the sum of time intervals dt needed to pass the distances dr: $dt = G^{-1}dr$. Because G depends on the x coordinate only and $dr = dx \cos \phi$, time t can be expressed as the following integral:

$$t = (\cos \phi)^{-1} \int_{x_0}^{x} G(x')^{-1}\, dx' \tag{5}$$

where $x = x_0 + R(\phi,t)\cos \phi$. Equation (4a) can, therefore, be written in the following form:

$$E(x_0, t) = 2 \int_{x_0 - R(\pi,t)}^{x_0 + R(0,t)} D(x)(x - x_0)\tan \phi\, dx \tag{6}$$

where $R(0,t)$ and $R(\pi,t)$ are expressed by eq. (5) for $\phi = 0$ and $\phi = \pi$. After substitution of $\tan \phi$ with $[(\cos \phi)^{-2} - 1]^{0.5}$, where $\cos \phi$ is calculated from eq. (5), eq. (6) assumes the following form:

$$E(x_0, t) = 2 \int_{x_0 - R(\pi,t)}^{x_0 + R(0,t)} D(x)|x - x_0| \times \left\{ t^2 \left[\int_{x_0}^{x} G(x')^{-1}\, dx' \right]^{-2} - 1 \right\}^{0.5} dx \tag{7a}$$

For the three-dimensional crystallization, E can be derived in a similar way:

$$E(x_0, t) = \pi \int_{x_0 - R(\pi,t)}^{x_0 + R(0,t)} D(x)(x - x_0)^2 \times \left\{ t^2 \left[\int_{x_0}^{x} G(x')^{-1}\, dx' \right]^{-2} - 1 \right\} dx \tag{7b}$$

For the introduction of the time dependence of the primary nucleation rate, $F(x,t')$, the area S (t',t) is defined for each value of the nucleation time t'. Equation (5) has to be modified in the following way:

$$t - t' = (\cos \phi)^{-1} \int_{x_0}^{x} G(x')^{-1}\, dx' \tag{8}$$

where $x = x_0 + R(\phi,t',t)\cos \phi$ and $R(\phi,t',t)$ is equal to the radius toward point A at time t of a spherulite nucleated at the circumference of $S(t',t)$, at angle ϕ,

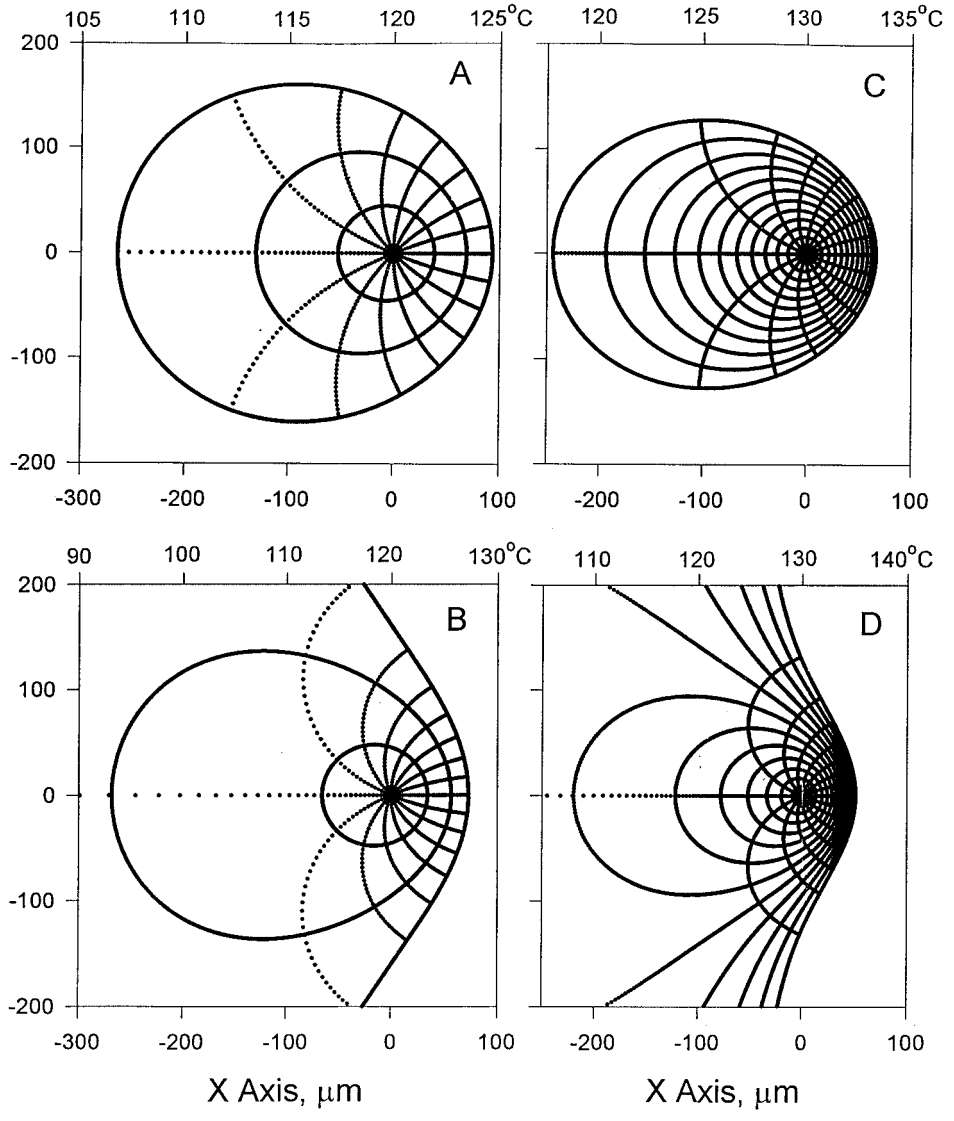

Figure 2 Spherulite shapes predicted by the variable-growth-direction model for (A,C) $\Lambda = 50$ K mm^{-1} and (B,D) $\Lambda = 100$ K mm^{-1}: (A) nucleated at 120°C, (B) nucleated at 120°C, (C) nucleated at 130°C, and (D) nucleated at 130°C. The positions of spherulite growth fronts are plotted in 1-min intervals. Lines emanating from the centers indicate the growth directions.

and at time t'. E is calculated by the integration of $F(x,t')$ over $S(t',t)$ followed by the integration of the result over $0 < t' < t$. Therefore, for the two- and three-dimensional processes, $E(x_0,t)$ is expressed by the following formulas:

$$E(x_0, t) = 2 \int_0^t \int_{x_0-R(\pi,t',t)}^{x_0+R(0,t',t)} F(x, t')|x - x_0| \times \left\{ (t - t')^2 \left[\int_{x_0}^{x} G(x')^{-1}\, dx' \right]^{-2} - 1 \right\}^{0.5} dx\, dt' \quad (9a)$$

$$E(x_0, t) = \pi \int_0^t \int_{x_0-R(\pi,t',t)}^{x_0+R(0,t',t)} F(x, t')(x - x_0)^2 \times \left\{ (t - t')^2 \left[\int_{x_0}^{x} G(x')^{-1}\, dx' \right]^{-2} - 1 \right\} dx\, dt' \quad (9b)$$

where $R(0,t',t)$ and $R(\pi,t',t)$ are described by eq. (8).

For constant G, D, and F, the expressions for $E(t)$ are obtained from eqs. (7) and (9): $\pi D(Gt)^2$, $(4/3)\pi D(Gt)^3$, $\pi Ft(Gt)^2/3$, and $\pi Ft(Gt)^3/3$ (known from the Avrami and Evans theory).

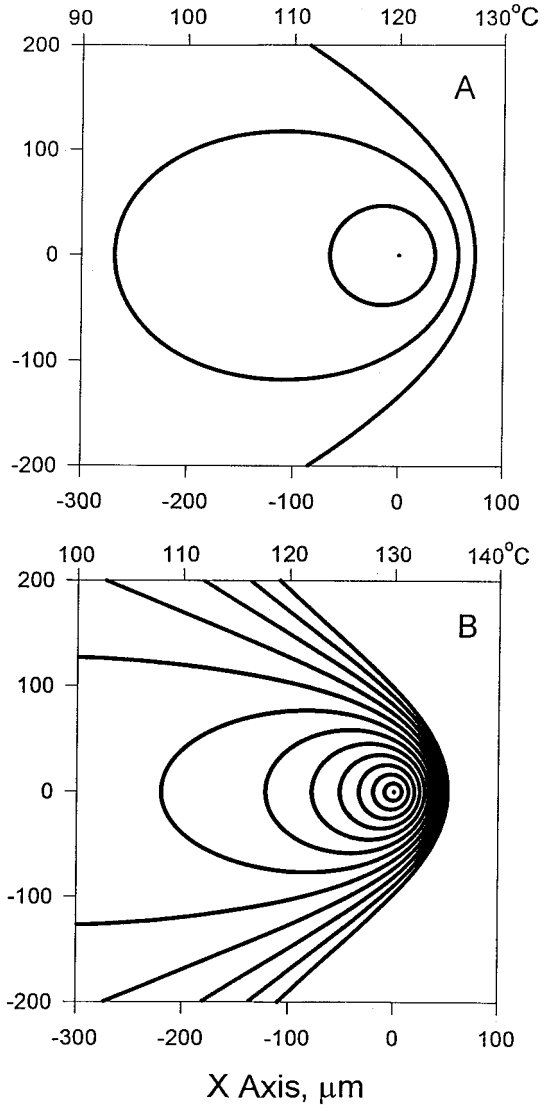

Figure 3 Spherulite shapes predicted by the radial-growth model for $\Lambda = 100$ K mm^{-1}: (A) nucleated at 120°C and (B) nucleated at 130°C. The positions of spherulite growth fronts are plotted in 1-min intervals.

RESULTS OF MODELING

The computer-simulated spherulites and spherulitic patterns are shown in Figures 2–6. In all cases, the temperature gradient is parallel to the x axis, and the temperature, T, increases from the left to the right. Figure 2 shows examples of spherulites for the temperature gradient, Λ, equal to 50 K and 100 K mm^{-1} with centers located at 120 and 130°C. The temperature gradient results in the spherulite shape anisotropy, which increases with time. Lamella growth directions, normal to the growth front, turn toward the hotter side. Therefore, the hotter part of the spherulite flattens and becomes composed of nearly parallel lamellae. This tendency is enhanced by the increase in Λ and T. The radial-growth model leads also to the anisotropy of spherulite shapes, as shown in Figure 3, although the spherulites are flatter in polar regions. This deviation increases with the time of growth and is more pronounced at higher T and higher Λ.

The shapes of interspherulitic boundaries depend on the temperature, temperature gradient, positions of spherulite centers, and distances between them. Only spherulites with centers at the same isotherm develop a straight line boundary equally distant from both spherulite centers. In Figure 4(a,b), the interspherulitic boundaries are shown as predicted by the variable-growth-direction model. The boundary between spherulites nucleated on the line parallel to the temperature gradient is curvilinear and symmetrical with respect to this line. In other cases, the symmetry is not preserved. The boundaries bend toward higher T, as-

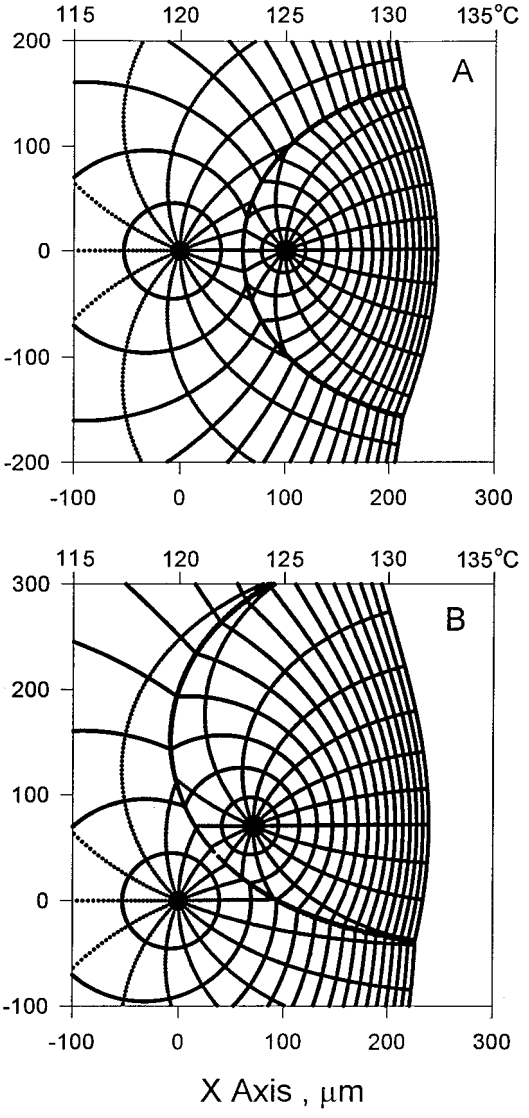

Figure 4 Shapes of interspherulitic boundaries predicted by the variable-growth-direction model for $\Lambda = 50$ K mm^{-1}: (A,B) various positions of spherulite centers.

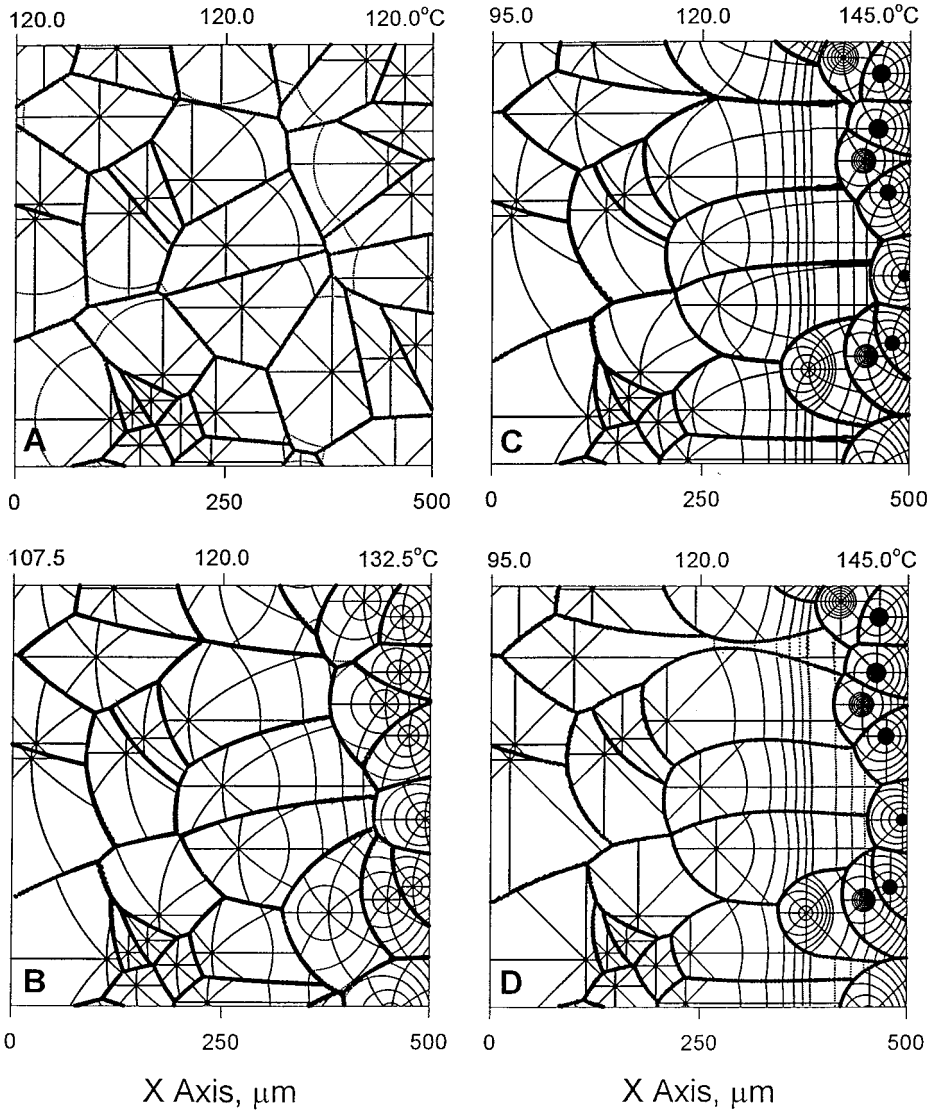

Figure 5 Computer-simulated development of spherulitic patterns with $D = 100$ mm^{-2}: (A) isothermal conditions; (B) $\Lambda = 50$ K mm^{-1}, variable-growth-direction model; (C) $\Lambda = 100$ K mm^{-1}, variable-growth-direction model; and (D) $\Lambda = 100$ K mm^{-1}, radial-growth model. In parts A and B, growth-front positions are plotted in 2-min intervals; in parts C and D, growth-front positions are plotted in 2-min intervals for the first 12 min and later in 12-min intervals.

suming finally the direction parallel to the temperature gradient. The spherulites nucleated on the colder side tend to occlude the neighbors nucleated on the hotter side. The curvature of the boundary increases also with the distance between spherulite centers. The boundary is always closer to the center of the spherulite nucleated at higher T. These tendencies are enhanced in the higher T and Λ.

The influence of the temperature gradient on the evolution of the spherulitic pattern is demonstrated in Figures 5 and 6. The directions of the growth of spherulites and the positions of the spherulite growth fronts in subsequent time intervals are also marked in these figures. In Figure 5, the structures composed of spherulites propagating from identically localized nuclei are shown: the Voronoi diagram obtained for isothermal conditions, the pattern predicted by the variable-growth-direction model, and, for comparison, the pattern obtained on the basis of the radial-growth model. The temperature gradient alters the spherulitic pattern even if temperature-independent nucleation density is assumed. The effect increases with increases in both Λ and T. Although the spherulites grow faster toward the sample colder side, they soon impinge on others. They can still grow toward the hotter side; this results in their elongated shapes and in the formation of a joint growth front. The lamellae within this front tend to assume the direction parallel to the temperature gradient. The front flattens with time and occludes spherulites nucleated ahead of it; this is espe-

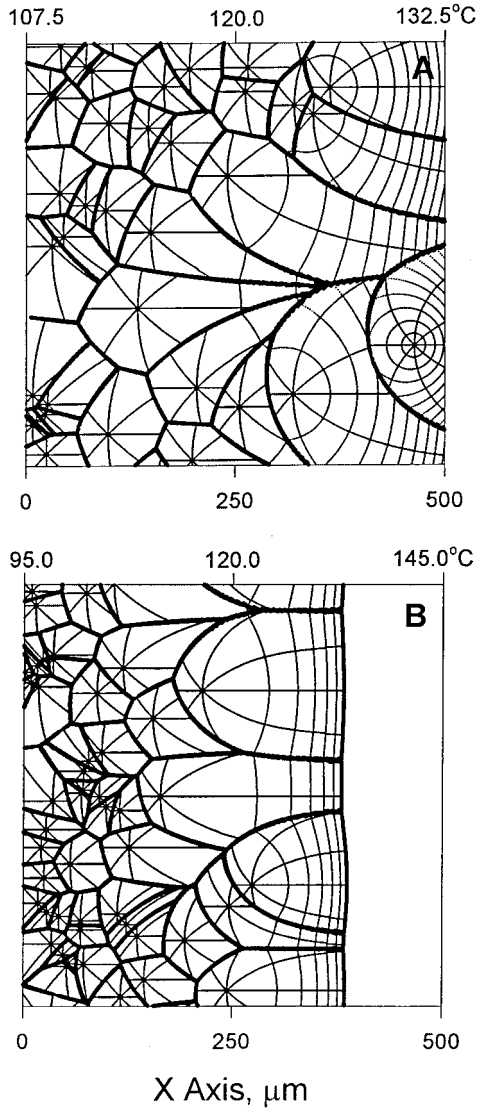

Figure 6 Computer-simulated samples with a nucleation density proportional to the growth rate ($D = G \times 1.33 \times 10^5$ s mm^{-3}): (A) $\Lambda = 50$ K mm^{-1} and (B) $\Lambda = 100$ K mm^{-1}; the variable-growth-direction model, growth-front positions are plotted in 2-min intervals.

cially well seen for $\Lambda = 100$ K mm^{-1}. The pattern generated with the radial-growth model (not shown here) for $\Lambda = 50$ K mm^{-1} is nearly identical to the pattern evolved with the variable directions of growth. The differences between patterns generated by the different models can be clearly seen for $\Lambda = 100$ K mm^{-1}, especially in the parts of samples containing elongated spherulites. Although the variable-growth-direction model predicts the boundaries parallel to the temperature gradient, the radial-growth model leads to further bending of such boundaries. The analysis of sets of pictures similar to those shown in Figure 4 indicate that the deviations between the shapes of boundaries calculated on the basis of different models may appear also for lower Λ, such as 50 K mm^{-1}; however, this would have required a longer time than the time needed for the accomplishment of crystallization in the sample. Nevertheless, both models predict similar shapes and positions of flat growth fronts formed by many spherulites on the hotter side of the sample.

In Figure 6(a,b), the patterns with temperature-dependent D, proportional to G (a type of isokinetic case), generated on the basis of the variable-growth-direction model are demonstrated. D in the central part of simulated samples, near the 120°C isotherm, is the same as in samples shown in Figure 5(a–c). In addition to the morphology changes seen in Figure 5, the enlargement of spherulite sizes with the local temperature increase is observed in Figure 6. At low T, however, the interspherulitic boundaries are affected only a little by the temperature gradient; the effect is weaker than that visible in Figure 5(b,c) because of the shorter distances between the spherulite centers. The spherulites nucleated in the colder part of a sample extend toward the hotter side, where the nucleation is weak, which is especially visible for $\Lambda = 100$ K mm^{-1}. The conversion of the melt into spherulites occurs via an advancement of the growth front formed by the spherulites nucleated in the colder part of the sample.

The conversion degree/time dependencies calculated according to eq. (7a) for the isotherms at 120 and 125°C are plotted in Figure 7(a,b) for a range of Λ values for two constant D values, 100 and 1000 mm^{-2}, and also for $D = B \times G$. In the latter case, the following values of B were chosen: 1.33×10^5, 1.33×10^6, 2.86×10^5, and 2.86×10^6 s mm^{-3}. The first two values of B result in $D = 100$ mm^{-2} and $D = 1000$ mm^{-2} at 120°C, whereas the last two give $D = 100$ mm^{-2} and $D = 1000$ mm^{-2} at 125°C, respectively. The conversion degree/time dependencies for isothermal crystallization are also drawn for comparison. The data points delivered by the computer simulations based on the variable-growth-direction model and the radial-growth model, marked in these plots, follow the curves calculated according to eq. (7a). This indicates that although the assumption of radial growth of spherulites may lead to an erroneous prediction of the spherulitic pattern, especially for large temperature gradients, it still allows us to calculate the correct conversion degree of the melt into spherulites even for Λ as high as 200 K mm^{-1}.

The temperature gradient speeds up the conversion of the melt into spherulites. This depends, however, on the local temperature, the value of the gradient, and the nucleation density. For $D = 100$ mm^{-2} (average spherulite radius = 56 μm) the conversion of the melt into spherulites becomes markedly faster for $\Lambda \geq 50$ K mm^{-1}, whereas for $D = 1000$ mm^{-2} (average spherulite radius = 18 μm), $\Lambda \geq 200$ K mm^{-1} is

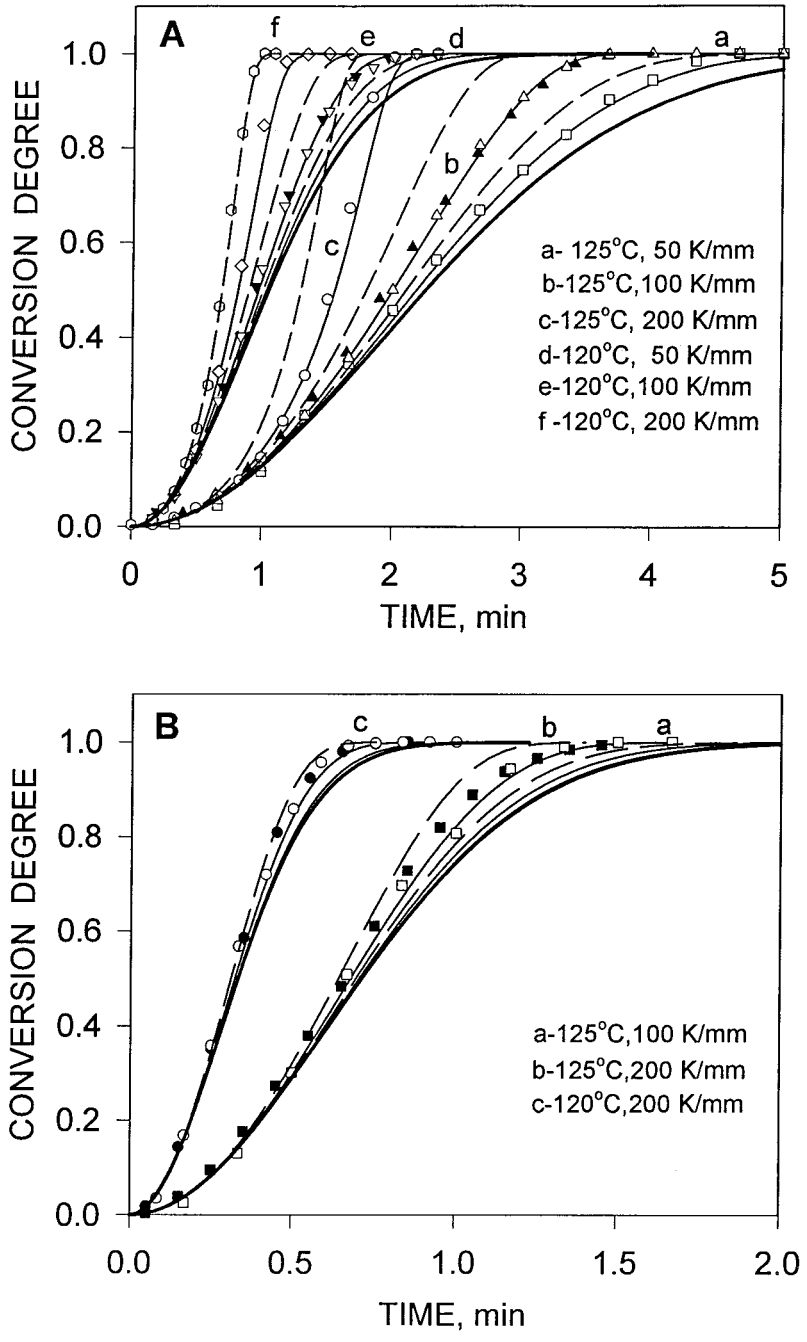

Figure 7 Conversion degree against time during gradient crystallization at isotherms of 120 and 125°C and during isothermal crystallization at 120 and 125°C (thick, solid lines), as predicted by the probabilistic model. (A) The solid lines indicate a constant nucleation density ($D = 100\ \text{mm}^{-2}$), and the dashed lines indicate a nucleation density proportional to the growth rate ($D = B \times G$, where B values give $D = 100\ \text{mm}^{-2}$ at 120 and 125°C). (B) The solid lines indicate $D = 1000\ \text{mm}^{-2}$, and the dashed lines indicate $D = B \times G$ (where B values give $D = 1000\ \text{mm}^{-2}$ at 120 and 125°C). Symbols denote the results of computer simulations based on the radial-growth model (filled) and the variable-growth-direction model (open).

needed for a marked acceleration of the conversion. Therefore, it can be concluded that a temperature difference of several degrees per a distance equal to an average spherulite diameter is necessary to influence the conversion rate. The temperature dependence of the nucleation density leads to further enhancement of the conversion, which indicates the importance of the nucleation in the colder part of the sample during the crystallization in the temperature gradient. The elevation of the nucleation density weakens the effect.

In Figure 8(a), a computer-simulated iPP film 11 μm thick crystallizing in a gradient of 35 K mm^{-1} is dem-

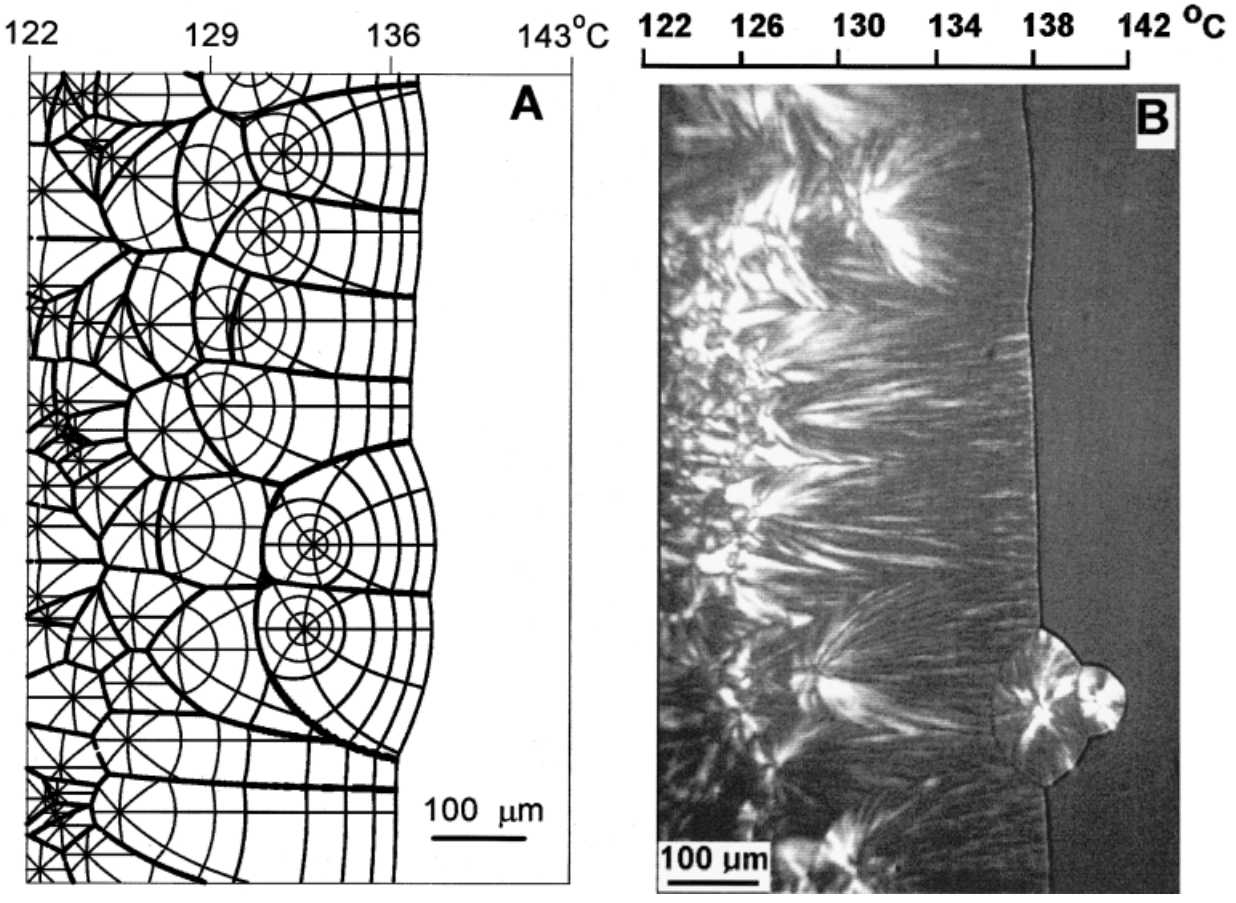

Figure 8 Spherulitic patterns in iPP films during crystallization in the temperature gradient of 35 K mm^{-1}. (A) A computer-simulated, 11-μm-thick iPP film is shown. All parameters were used as measured for iPP (Polysciences; M_w = 220,000); the nucleation density was calculated according to eq. (3). Positions of the crystallizing front were plotted in 4-min intervals during the first 12 min and later in 12-min intervals. (B) A polarizing micrograph of iPP crystallizing film (Polysciences; M_w = 220,000) is shown.

onstrated. The simulation was based on the variable-growth-direction model, whereas the temperature-dependent nucleation density was calculated according to eq. (3). In Figure 8(b), the micrograph of an iPP film (Polysciences; M_w = 220,000) crystallizing in the gradient of 35 K mm^{-1} is shown for comparison. The experimental details of gradient crystallization are described in ref. 4. The same morphological features are visible in both pictures, indicating the correctness of the computer simulation. In Figure 9, the time dependencies of the conversion rate at isotherms at 128, 132, and 134°C for Λ = 37 K mm^{-1} and at 134.5°C for Λ = 35 K mm^{-1} are plotted as predicted by the probabilistic model for iPP films 11 μm thick. The conversion degree during the isothermal crystallization at respective temperatures is also plotted for comparison. The data points obtained from the computer simulation based on the variable-growth-direction model follow the curves based on eq. (8a). Equation (3) was applied for the calculation of the nucleation density used in the modeling. The experimental data points from ref. 4 agree well with the theoretical predictions of the acceleration of the conversion of the melt into spherulites.

CONCLUSIONS

The computer simulation of spherulite growth permitted us to visualize the evolution of spherulitic patterns during crystallization in the temperature gradient. It showed the anisotropy of spherulite shapes, the curvature of interspherulitic boundaries, the variations of the directions of lamella growth, and the development of joint growth front in later stages. It enabled us to predict the changes in the spherulitic structure and in the overall kinetics of the conversion of the melt into spherulites. The changes in the spherulitic structures predicted by computer simulation based on the variable-growth-direction model agreed well with the experimental observations.

The computer simulation allowed us to estimate the possible error introduced by the assumption of radial

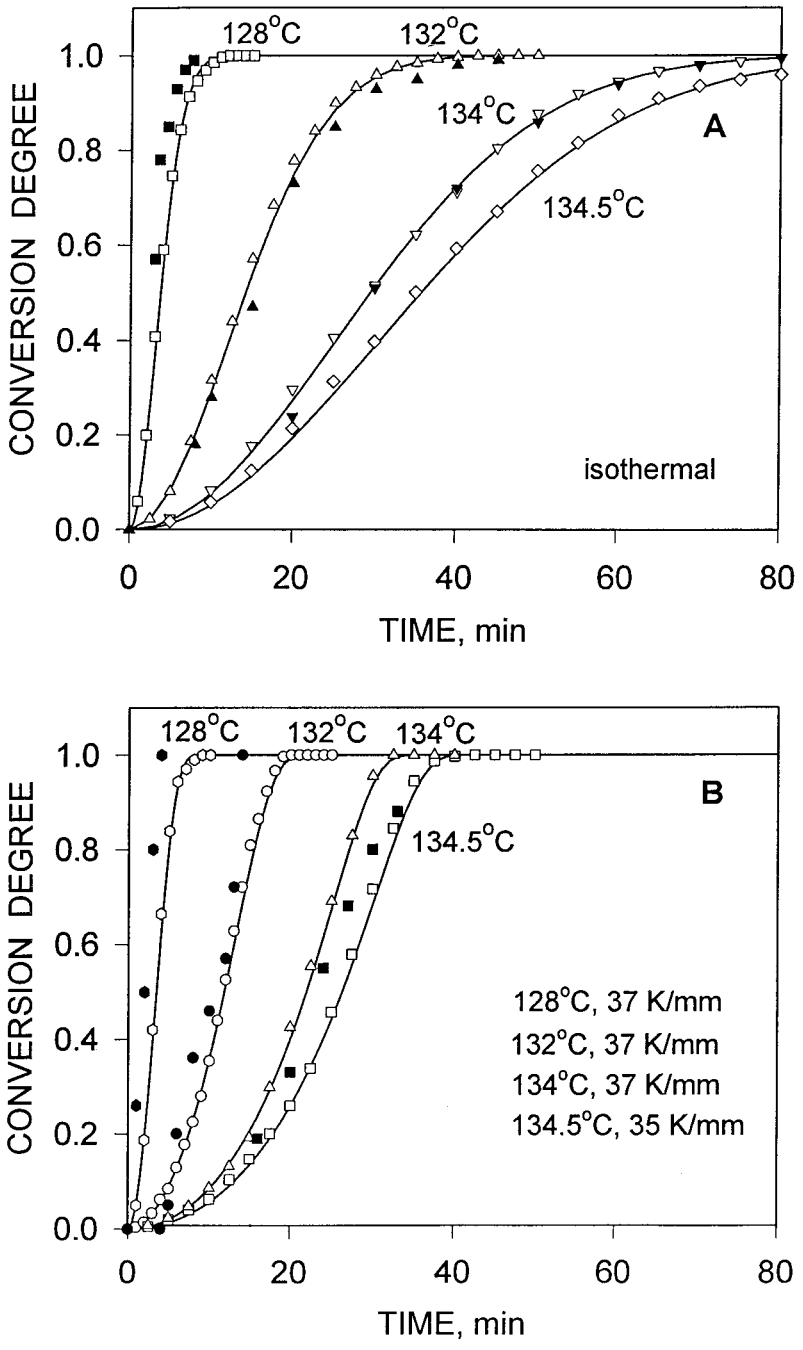

Figure 9 Comparison of the prediction of the probabilistic model (lines) and the results of computer simulation based on the variable-growth-direction model (open symbols) with the experimentally measured time dependence of the conversion degree (filled symbols) for iPP films during isothermal and gradient crystallization (experimental data from ref. 4).

growth—the basis of the existing theories of overall crystallization. In simulation of crystallization in the temperature gradient of 100 K mm^{-1}, it did not significantly affect the outlines of the spherulitic growth front or, therefore, the conversion degree. The probabilistic model was also described and allowed the prediction of the conversion degree of the melt into spherulites in the steady unidirectional temperature gradient. The computer simulation confirmed the usefulness of the probabilistic model despite the assumption of radial spherulite growth made during derivation of the analytical formula. Both the computer simulation and the probabilistic model allowed the prediction of the conversion of the melt into spherulites during the gradient crystallization. The prediction of the probabilistic model, supported by the results of the computer simulation, showed the acceleration of the conversion of the melt into spherulites in

the temperature gradient. It could be explained with the help of computer simulation as the result of the contribution of spherulites advancing from the colder part of a sample to the conversion rate. The alterations in the spherulitic structure and overall kinetics of conversion were enhanced by the higher temperature, the higher temperature gradient, and the weaker nucleation of spherulites. The temperature increment caused a larger relative change in the iPP spherulite growth rate at the higher temperature. This implied more anisotropic growth of spherulites at elevated temperatures and more pronounced changes in lamella growth directions and in the shapes of interspherulitic boundaries. The weaker nucleation of spherulites increased distances between spherulite centers, allowing for longer crystallization and, therefore, the enhancement of spherulite shape anisotropy. It allowed also for a more significant contribution of spherulites from the colder part of a sample to the conversion rate, which accelerated the polymer solidification.

References

1. Keith, H. D.; Loomis, T. C. J Polym Sci Polym Phys Ed 1984, 22, 295.
2. Lovinger, A. J.; Chua, J. O.; Gryte C. C. J Polym Sci Part B: Polym Phys 1977, 15, 641.
3. Schulze, G. E. W.; Naujeck, T. R. Colloid Polym Sci 1991, 269, 695.
4. Pawlak, A.; Piorkowska, E. Colloid Polym Sci 2001, 279, 939.
5. Evans, U. R. Trans Faraday Soc 1945, 41, 365.
6. Avrami, M. J Chem Phys 1939, 7, 1103; 1940, 8, 212; 1941, 9, 177.
7. Kolmogoroff, A. N. Isv Akad Nauk 1937, 3, 355.
8. Piorkowska, E.; Galeski, A. J Appl Polym Sci 2002, 86, 1363.
9. Galeski, A. J Polym Sci Polym Phys Ed 1981, 19, 721.
10. Grenier, D.; Prudhomme, R. E. J Polym Sci Polym Phys Ed 1980, 18, 1655.
11. Billon, N.; Escleine, J. M.; Haudin, J. M. Colloid Polym Sci 1989, 267, 668.
12. Ozawa, T. Polymer 1971, 12, 150.
13. Escleine, J. M.; Monasse, B.; Wey, E.; Haudin, J. M. Colloid Polym Sci 1984, 262, 366.
14. Billon, N.; Haudin, J. M. Colloid Polym Sci 1989, 267, 1064.
15. Billon, N.; Magnet, C.; Haudin, J. M.; Lefebvre, D. Colloid Polym Sci 1994, 272, 633.
16. Piorkowska, E.; Galeski, A. J Phys Chem 1985, 9, 4700.
17. Piorkowska, E.; Galeski, A. J Polym Sci Polym Phys Ed 1985, 23, 1273.
18. Piorkowska, E. J Chem Phys 1995, 99, 14007; 1995, 99, 14016; 1995, 99, 14024.
19. Piorkowska, E. Colloid Polym Sci 1997, 275, 1035; 1997, 275, 1046.
20. Lovinger, A. J.; Gryte, C. G. J Appl Phys 1976, 47, 1999.
21. Schulze, G. E. W.; Naujeck, T. R. Colloid Polym Sci 1991, 269, 689.
22. Swiminarayan, S.; Charbon, Ch. Polym Eng Sci 1998, 38, 634.
23. Charbon, Ch.; Swiminarayan, S. Polym Eng Sci 1998, 38, 644.
24. Clark, E.; Hoffman, J. D. Macromolecules 1984, 17, 878.
25. Pawlak, A.; Piorkowska, E. J Appl Polym Sci 1999, 74, 1380.
26. Nowacki, R.; Kolasinska, J.; Piorkowska, E. J Appl Polym Sci 2001, 79, 2439.
27. Pawlak, A.; Galeski, A. J Polym Sci Part B: Polym Phys 1990, 28, 1813.
28. Marsaglia, G.; Zaman, A. Ann Appl Prob 1991, 1, 462.
29. von Neumann, J. Natl Bur Stand Appl Math 1951, 12, 36.